ORIGINAL PAPER

Experimental analysis of tool geometry and tool rotation in SPIF process on AA7075-O alloy using ML and ANN approach

Parveen Kumar[1] · Hari Singh[1]

Abstract

Single Point Incremental Forming (SPIF) is a novel and die-less variant of Incremental Sheet Forming (ISF) which directly exempts the use and involvement of dedicated punch and dies. This is an agile and flexible methodology that directly saves energy and materials making the forming method ready for sustainable production. The estimation and analysis of forming force can assure the safe utilization of forming setup to perform the SPIF operation for the designed process conditions and materials. Artificial Neural Networks (ANN) models stimulate the Machine Learning (ML) techniques in computing the rendition and superiority by using pertinent and relevant input factors. Consequently, ANN-based techniques have been explored for SPIF process, to enhance the employability and suitability of the SPIF process to the mainstream of manufacturing industries. The presented work is to explore and estimate the axial peak forces during the SPIF process by using an experimental campaign and ML methodology. A comparison has been made between the actual, predicted values, and accuracy has also been analyzed to measure the efficiency of current model. The results delineate that the ANN model outperforms the other ML models with an accuracy of approximately 98%.

1 Introduction

Batch-type and customized manufacturing approaches have been considered as the latest aspects to upgrade the business of manufacturing sectors due to the cutting-edge requirements of the customers. Manufacturing of the complex and intricate shapes of components can be economical for customized and batch-size production when the reduced lead time and involved cost. Moreover, amount of wastage of material is minimum in forming operations. In conventional sheet forming operations, dedicated die-sets are required to accomplish the forming process that turns into a hindrance for persuading the requisite of customized manufacturing [1]. Moreover, the larger forming forces are needed, during conventional forming, to execute the deformation that in turn raises the requirement of the bigger machinery and forming set-up. The implementation of the bigger machinery directly

makes the forming operations costlier if volume of production does not reach the breakeven level of the operation [2]. Also, substantial growth in the obsolescence of traditional forming-methods has produced the demand for flexible and agile techniques for manufacturing user-ready components in the global market. ISF has the potential to escalate the insurrection in the field of rapid manufacturing due to its agility and flexibility. ISF yielded in the starting of the current century and is fascinating the researchers as a choice of green manufacturing without using dedicated punches and dies [3–5]. Moreover, ISF overcomes the issues that are encountered in manufacturing field because of the non-availability of die-sets of old machinery such as fuselage parts of old aircraft and sheet metal components of vintage cars, etc. Also, ISF exhibits the potential to manufacture the end-user parts with almost no-wastage, remarkable surface quality, considerable strength, and lower tolerances. In ISF, the deforming load for the sheets are considerably lower as compared to other sheet forming techniques which enable the use of quite small-size and light-weight machines to accomplish the process. Hence, the breakeven point of this die-less process is achieved by manufacturing a smaller number of parts due

✉ Parveen Kumar
  parveenkumarme@gmail.com

1   Department of Mechanical Engineering, National Institute of
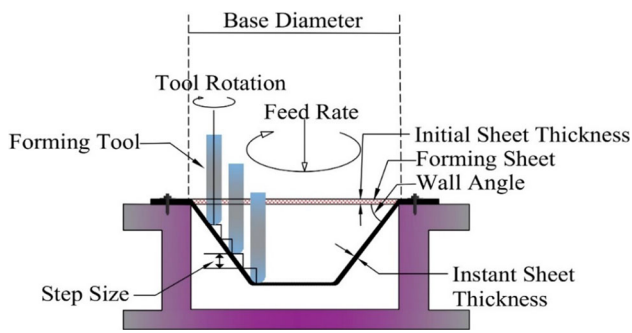   Technology, Kurukshetra, Haryana 136119, India

Fig. 1 Illustration of SPIF method

Fig. 2 Force measuring approach

to the lower cost of machines and tools of small capacity involved in it. The customized parts can also be economically produced by this process which enables the greater productivity, higher flexibility, lightweight parts, and higher accuracy [6, 7]. The postulate of the ISF consists of deforming the material, clamped in the fixture, progressively with the maneuver movement of a forming punch which is supervised by the NC mechanism [8]. The forming tool is clamped on a rotating spindle and provided the downward motion according to step size [9–11]. SPIF (Fig. 1) is a viable and novel variant of ISF which exempts the involvement of dies to produce the parts and is also known as "die-less forming process" or "negative incremental forming". SPIF directly finds applications in various manufacturing sectors including medical, bio-medical, dental, aerospace, agriculture, automobile, and architecture.

In SPIF, the strain is purely local because very small amount of forming load is desired to manufacture the workpiece. The requirement of lower amount of force decreases the consumption of energy and power for executing this operation. Therefore, small size of machines can perform the process efficiently [12]. Hence, the amount of maximum force that is desired to deform the sheet material under certain process conditions and materials, delineate the capacity of forming machinery. Therefore, secure and effective employment of experimental setup is secured by estimating and investigating the maximum force values [13]. During this operation, the force values are generally measured by mounting the force dynamometers either on the forming tool or between the ISF fixture and machine table. Most of the researchers [14–26] have used a later method (in which a load cell or force dynamometer is fixed between the fixture and machine table) as shown in Fig. 2. Yang et al. [14] investigated the forming load by changing the values of the step depth and temperature of sheet material (PEEK) and produced truncated pyramidal shapes of varying wall angle and constant wall angle.

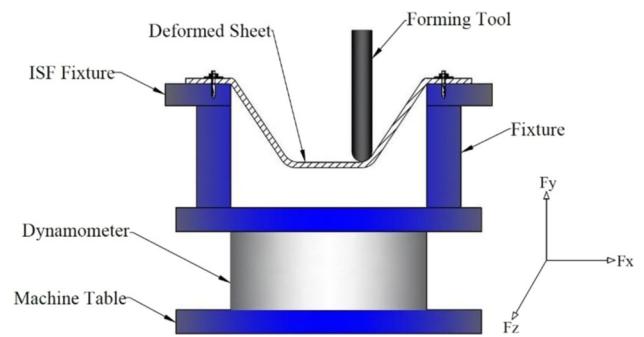They found that deforming load increased drastically when the step size was increased for all shapes of pyramidal frustums. Oraon et al. [15] observed the impact of input variables and developed the ANN model. They found that the combination of minimum step depth, reduced forming angle and lower sheet thickness resulted in minimum deforming force. They used feed-forward back-propagation algorithm to train the model. This model was limited to estimate load values for AA-3003-O and Cu67Zn33 sheets only. Bansal et al. [16] developed a model to estimate the deforming load taking contact area into consideration and made a comparative analysis for single stage and multi stage approaches of forming for Al 5052 and Al 3003 sheets. The proposed model was able to give results similar to the results produced by experimental campaign. Suresh et al. [17] analyzed impact of input variants for AA-1100 sheets by an experimental campaign and observed that step size, punch radius and forming angle control the deforming forces significantly. It was also observed that the magnitude of deforming load was greater in initial stage of forming operation and then became constant. Liu et al. [18] offered a theoretical approach for estimating the real values of deforming load in three directions which was based on assuming the stress in the forming zone and then it was processed according to experimental scenario and deformation behavior of material. The experiments were performed on AA-1050-O sheets for fabricating the pyramidal frustums of 55° forming angle. They observed that the model successfully predicted the load values with an error of 18%. Wernicke et al. [19] proposed an approach to reduce the desired deforming load in incremental forming of gears by using the mechanism of electroplastic effects for DC04 and HSM 700 HD sheets numerically. They observed that required load for given process condition was found to reduce up to 55%. They also developed an analytical model for estimating the current density which was dependent on actual and numerical data. Hussain et al. [20] reported the significance of stretching force and impact variables on the wall curling of the pyramidal frustums produced from Cu/Steel composite. A meaningful correlation, between the curling of parts and stretching force with other impact variables, was also investigated. They observed that the curling effect was lowered when the stretching force values were increased.

It was also found that the curling effects reduced with the employment of high punch radius, low forming angle. Liu and Li [21] also used ANN model to estimate the deforming load for various step size and the experimental values was considered for training of model. They formed the pyramidal frustums from AA 7075 sheets for this purpose. They also offered an optimization approach for reducing the errors during estimation using a hybrid objective function. The developed model was able to estimate the tangential load values significantly. Kumar et al. [22] optimized the process conditions in terms of forming force taking the Taguchi technique into account for AA 6063 and AA 2024 sheets. A statistical approach was offered to forecast the desired deforming load. This model was also verified with additional experimental campaign. An increase of 14.20% was noticed in peak load value when a forming tool of flat-end shape was used as compared to the forming tool of the hemispherical shape of the same diameter. Kumar and Gulati [23] also offered a model for forecasting the deforming load taking the Taguchi technique into account for AA 2014 sheets. Profile and spiral tool paths were used for manufacturing the truncated cones. The rise in step size, punch radius and thickness of sheet resulted in raising the deforming load value to a crucial level. Chang et al. [24] estimated the deforming load using an analytical approach which was further verified by the results obtained from experimental work on AA 5052 and AA 3003 alloys sheets.

Previous work [6, 22, 23, 26] also reports that the vertical component of deforming load (Fz) is greater than the horizontal components (i.e. Fx and Fy; see Fig. 2 for load components). Hence, measurement of maximum vertical forces, for performing the SPIF process, may secure the effective utilization of experimental setup. Also, the investigation of the relationship between input variables and forming forces can open the window to estimate the failures of parts, machinery, and forming processes efficiently. Furthermore, the estimation of forming forces can ensure the prediction of power to be consumed by the forming machine and controlling the process on-line.

The conventional models may not explain the nonlinear correlation between the impact variables and the deforming load during SPIF. The Machine Learning (ML) models [27–38] are able to develop the nonlinear and complex correlation between input variables and output factors as an alternative and effective solution. The ML models can be utilized effectively for optimizing the response of the process by setting suitable input parameters. Furthermore, data samples can be used to train the ML model which comprises dependent variables and the independent variable (output or response). In SPIF, the implementation of ML models can help the researchers and investigators to minimize required resources viz. power consumption, forming time and cost of the process by estimating the required deforming load. These models can also be utilized to control and monitor the process on-line and prevent the failure of hardware. It has been observed from the literature that artificial intelligence- based models have the potential to estimate the output in manufacturing processes [37, 39–41].

Li et al. [47] investigated and predicted heating effects in HA-ISF process numerically on aluminum alloys and high precision FEM model was established for the forming region taking thermal conductance into account. Li et al. [48] also investigated effect of Molybdenum disulphide (MoS_2) on Ti-6Al-4V sheets using HA-ISF. A roller-ball ended deforming punch was employed in such a manner that the MoS_2 could reach the forming zone directly through the tool-end for decreasing the thermal stresses and expansion. The deforming loads were found to decrease with the use of MoS_2 as a lubricant. Najm et al. [49] investigated the effects of various punch shapes, punch materials and punch radii on the pillow effects of the formed components from the AlMn1Mg1 alloy sheets experimentally. They further developed a ML model to predict the pillow effects using the experimental data for the training purpose of the ML models. To perform forming force prediction in SPIF, intense literature survey is carried out. Table 1 represents the different models used for predicting the deforming load for different materials during SPIF technique.

ML is the trending and widely used approach for predicting the response to complex problems because of computer-based algorithms that train the computer to learn through the process and improve the accuracy of output automatically. Through ML, a system learns from its experience like human learns without programming explicitly. Therefore, ML models have been explored to forecast the nature and level of maximum load value in this operation. The current work explores the supervised learning techniques of machine learning to predict the maximum axial forming force (Fz_max.) during the SPIF process. In this work, three supervised-learning techniques namely Support Vector Machine (SVM), Random Forest Regression (RFR), and ANN have been considered based upon their merits and suitability of undertaken parameters and Design of Experiment (DOE). SVM regression has been employed with four different kernels to design four models viz. SVM–linear (model 1), SVM -Ploy (model 2), SVM–Gaussian Process (model 3) and SVM–RBF (model 4). Apart from SVM, the RFR (model 5) and ANN (model 6) models have also been designed and fine-tuned for the efficient prediction of the Fz_max in the SPIF process for the selected input factors and process conditions. Literature [27] also reports that the SVM technique is suitable for obtaining better results for a small sample size. All the models have been trained and tested on the experimental dataset to predict the axial peak force (Fz_max) to calculate the accuracy of training and testing. Thereafter, the

Table 1 Summary of literature published related to forming force prediction in SPIF

References	Model	Material	Input parameters	Computational time
Alsamhan et al. [46]	ANFIS, ANN, QR	AA1050	Punch radius, tool feed, step size, thickness of sheet	No
Liu and Li [21]	ANN	Al7075-O	Punch radius, forming angle, thickness of sheet, step size	No
Racz et al. [42]	ANFIS	DC04	Punch radius, tool rotation, tool feed, step depth	No
Jawale et al. [43]	ANN	AA1050-H14	–	No
Oraon and Sharma [44, 45]	ANN	AA3003-O, Cu67Zn33	Tool feed, tool rotation, step size, forming angle, sheet material, thickness of sheet	No
Current work	ANN SVM	AA7075-O	Tool shape, Spindle speed	Yes

Table 2 Chemical composition of AA7075-O sheets

Chemical composition (weight %)								
Al	Cr	Cu	Fe	Mg	Mn	Si	Ti	Zn
89.70	0.24	1.50	0.30	2.40	0.20	0.20	0.16	5.30

estimated values and actual experimental values of deforming load have been compared, and the accuracy of offered models has also been analyzed to measure the efficiency.

The main objective of proposed research is to explore and analyze the impact of tool rotation (spindle speed), tool shape, and their interactions on peak deforming load values for AA7075-O sheets. The interactions of these parameters have not been tested for the considered alloy and operation conditions during the SPIF process to the best of author's knowledge. Furthermore, machine learning techniques have also not been implemented to predict the maximum deforming loads for this alloy during the SPIF process so far. The machine learning techniques may provide a channel to scientists and researchers to predict the deforming load which offers an alternative economical, easy, and technology-based solution to the cumbersome experimental process of this die-less approach of forming. The material, taken under investigation (i.e., AA7075-O), has been widely accepted in sheet metal applications because of the various suitable characteristics such as lightweight, greater strength, and corrosion resistance. Table 2 represents the chemical composition of AA7075-O alloy used in the current study. The chemical compositions of the sheets of this alloy were identified using the optical emission spectrometer. In this work, two types of tool shape, viz. flat-end and hemispherical-end, of identical diameters (TD =12.50 mm) have been considered for investigating the deforming load as shown in Fig. 3 where R represents radius of hemispherical tool and r represents the
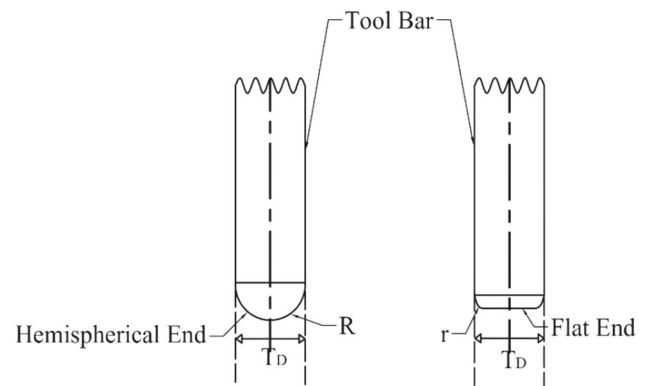
Fig. 3 Dimensional illustration of forming tool

side radius of flat-end tools. The flat-end tools of 2.30 mm and 3.40 mm side radius are denoted by Flatend#1 and Flatend#2 respectively, whereas radius of hemispherical tool is 6.25 mm and half of diameter of tool bar. The deforming tools were fabricated from the HSS rods. These tools were hardened and tempered before finishing their forming-end. To ensure the end-radii of these forming punches, Contracer CV-2100 was used. Table 3 depicts the full factorial scheme of experiments conducted in this work as DOE technique. Other impact factors were kept constant during experimentation examination as wall angle 64°, punch radius 6.25 mm, blank thickness 1.2 mm, step size 0.5 mm, feed rate 1500 mm/min and helical tool path.

Table 3 The impact factors varied for experimental examination

Impact factor	Value 1	Value 2	Value 3	Value 4
Tool shape	Flat end#1	Flat end#2	Hemispherical	–
Spindle speed (rpm)	1000	1500	2000	2500

2 Experimentation and methodology

The procedure of producing the designed components was started by designing a model of benchmark shape of a conical frustum (Fig.4a) of 62.5 mm upper radius and 75 mm forming height using the Solidworks® software. Afterward, the designed model was transferred to the Delcam™ software to generate the NC program and tool path instructions. The helical tool path (Fig.4b) was taken into consideration during this process. Thereafter, the forming tools were clamped in the collect of the machine, alternatively according to DOE, to perform the rotating action. Fig. 5 depicts the setup of experimental examination executed on a Vertical Machining Centre. The sheet of defined thickness was clamped in the SPIF fixture. The fixture was further firmly fixed on the machine table. The machine table was allowed to move in the x-axis and y-axis whereas the tool was given motion along the z-axis (vertical downward direction) so that a relative motion can be provided between the tool and sheet. Force dynamometer was installed below the fixture to experience the axial deforming load exerted by forming agent. The dynamometer was supported with a data acquisition system to record and amplify the signal of measured deforming load.

2.1 Development of support vector machine (SVM) model

SVM is one of the popular techniques which is used for solving supervised machine learning problems and suitable for regression and classification approaches. SVM algorithm trains the model using pairs of input output as training features or sample data [28]. The nonlinear SVM algorithm is used to predict the relationship between input data and dependent variables. SVM is built upon the hyperplane linear model concept which exploits the plane to find out the maximum margin. Hyperplane creates a decision boundary that helps to train the model by using input and output pairs of data samples. The number of input features determines the dimension of the hyperplane. In this research work, two input features have been used; hence the hyperplane is just a line as shown in Fig. 6a. In the n-dimensional space, we may produce several decision boundaries to separate the data points, but the SVM model requires us to choose the best decision boundary to classify the data points. The best separating line is called the hyperplane of SVM [29]. The hyperplane that

offers the maximum partition distance amongst the data samples is called an optimal hyperplane with maximum margin. An optimal hyperplane helps in achieving higher accuracy of the model. The separating hyperplane is a line that is used to divide data samples (Support vectors) with the decision boundary. Soft margin deals with the data points that are partitioned wrongly by separating the hyperplane. The soft margin permits margin violation while choosing a separating hyperplane that allows a few data points to settle on either side of the hyperplane and between the margin as depicted in Fig. 6a. SVM algorithm finds the closest points to the margin known as support vectors.

2.2 Development of random forest regression (RFR) model

Regression analysis is one of the popular machines leaning method that aspires to predict continuous output value using the independent input variables though their underlying relationship in data. To model higher order non-linear, the tree-based regression models have gained higher popularity owing to flexibility and higher interoperability. Traditionally, regression tree models are constructed in a two-phase process; (1) a recursive binary partitioning is performed to generate a tree structure, and (2) then pruning methods are employed to eliminate the insignificant leaves. The decision tree uses tree like structure as its name suggests, and predicts results. It start from the root node and ends at leaf node with a decision. A DT (Decision Tree) [30] can solve both the regression and classification problems. But a decision tree has high variance, therefore to reduce the variance, the decision trees are combined in parallel. Because of that the result of decision tree is not driven by only one decision tree but multiple decision trees that reduces variance. The principal idea behind combining of multiple decision trees is that the final out is determined by the multiple decision trees rather than depending only a single decision tree. Thus, Random Forest regression consists of multiple decision trees. The final predicted result is the mean of all outputs of the DTs in the forest. Random forest is a well-accepted algorithm for regression problems which is also known as an ensemble technique of machine learning [38]. The generic steps of random forest regression are: (a) In Random Forest regression, x number of random records are obtained from the dataset having i number of records, (b) Individual decision trees are constructed

Fig. 4 **a** Shape of conical frustum **b** Helical tool path adopted during forming

(a)   (b)
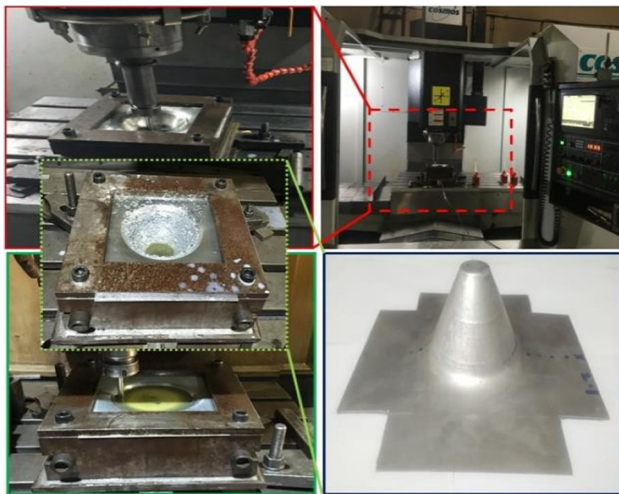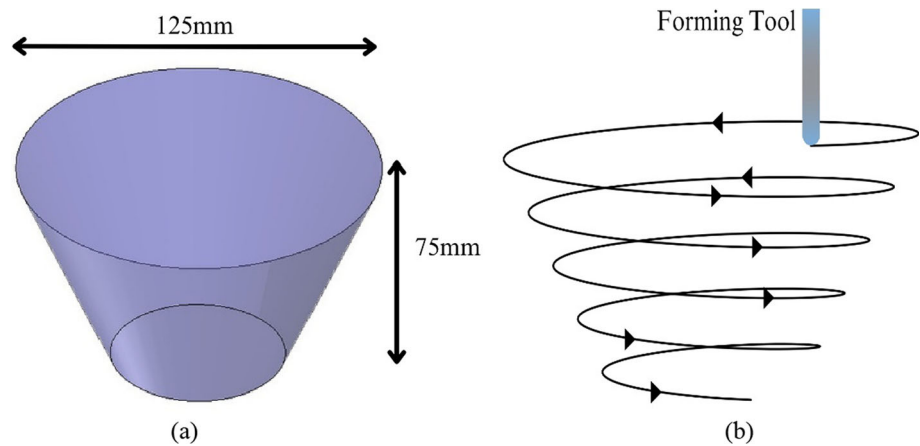
Fig. 5 The setup and process of experimental examination executed in this work

for each sample, (c) Every decision tree will produce an output, (d) The final output is generated on averaging outputs of DTs.

2.3 Development of ANN model

ANN is widely preferred by researchers and scientists over traditional approaches due to its nature of predicting the capabilities of complex linear and nonlinear input [32–34]. ANN is an information processing model that is inspired by the working of the human brain. ANN model mimics learning capabilities as a human learns. In this work, the ANN approach has also been used to train the model, and the training set has been extracted from the actual values of results. A generic architecture of an ANN is depicted in Fig. 6b. Figure 8 shows the design of ANN model for Prediction of Axial Peak Forces (Fz_max). The prime objective of designing this model (Figure 8) was to analyze the accuracy by forecasting the peak value of deforming load in this dieless

operation for the given levels of tool shape and spindle speed. The selected model comprises an input layer composed of two neurons as input variables i.e., spindle speed (x1) and tool shape (x2). The weight vector W is applied between each connection of neurons and random weights are applied in continuation. The weight indicates the robustness of an individual node. In addition to the two variables i.e. spindle speed (x_1) and tool shape (x_2), one additional input parameter bias b is also applied so that output is regulated along with the weighted sum of the input parameters to the neuron. A bias term allows to move or translate the activation function up or down. The ANN is used to predict the nonlinear relationship in the dataset and the real source of accuracy comes from the hidden layer. In this work, the hidden layer has used 50 neurons and the neurons of the hidden layer have not been visible to the outer world to implement the concept of abstraction. The hidden layer performs various computations for the given input factors (tool shape and spindle speed in this case) before passing to the output layer (y). Each neuron has the activation function which is processed on the given data for standardizing the output (y) which is forming force. The proposed model has utilized 50 epochs to train the model for predicting the output y (maximum forming forces).

In the generic form of ANN, each neuron in the hidden layers contains an activation / transfer function [f(a)]. The output of a neuron present in a hidden layer connected to n input layer neurons [32] can be expressed as:

$$y = f(a) \tag{1}$$

with, $a = \sum_{i=0}^{n} x_i W_i + b$

where x_i is ith independent variable and W_i is its corresponding weight, and b represents the bias term. The activation function of a neural network is illustrated by Fig. 7 [34].

The hidden layer is used to perform feature extraction and transformation. An activation function is applied on hidden layer for adjusting the weights of the neurons. This process

Fig. 6 a SVM with Soft Margin **b** Architecture of artificial neural network model

(a)　　　　　　　**(b)**
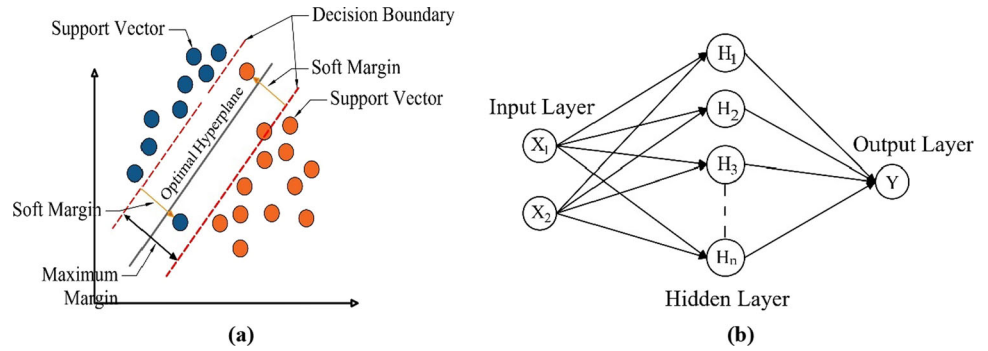
Fig. 7 Activation function of the ANN model
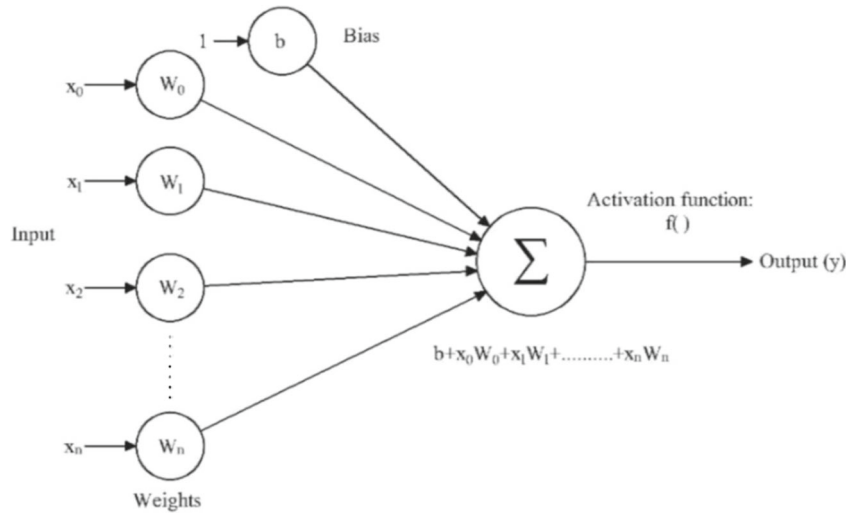
is followed by all the layers in the model until the predicted output (ŷ) is generated by the output layer in the first epoch. To calculate the error, the output

(y) and predicted ŷ is compared and an error value e is determined as per Eq. (2):

$$e = y - \hat{y} \tag{2}$$

To minimize the error e [32], the ANN model has used a multilayered feedforward backpropagation algorithm. The multilayered feed forward back propagation is neural network training algorithm which is used to improve the prediction accuracy. It consists of two steps: first step is to forward input values and second is calculate the error and propagate back to the previous layer in the network. It is also called backward propagation of errors in the neural network. The algorithm calculates the gradient of a loss function with respect to all the weights in the neural network. The fine-tuning of the weights reduces error rates and makes the model robust and reliable. The change in the hidden layer is a partial derivative for the change in weights which is expressed by Eq. (3).

$$y = \sum i \frac{\partial y}{\partial wi} \Delta wi + \frac{\partial y}{\partial b} \Delta b \tag{3}$$
$$for \ all \ i$$

Furthermore, the gradient descent is applied in each epoch to minimize the error, and learning rate α is applied for varying weights of the hidden layer neurons.
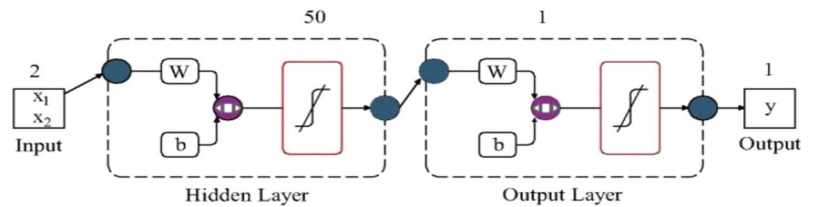
The relationship in the change in a learning rate α and change in error e expressed in Eq. (4):

$$\Delta a = -\alpha \Delta e \tag{4}$$

The change in the weights is computed by Eq. (5) and for the next epoch, the new weights wnew are calculated by Eq. (6):

$$\Delta w = w - \alpha \frac{\partial e}{\partial w} \tag{5}$$

$$w_{new} = w + \Delta w \tag{6}$$

Fig. 8 ANN model for prediction of axial peak forces (Fz_max)

Table 4 Experimental and predicted maximum axial force (Fz_max) for full factorial DOE

| Run	Spindle speed (RPM)	Tool shape	Experimental Fz_max (N)	Model I (SVM–Linear) Fz_max (N)	Model II (SVM–Poly) Fz_max (N)	Model III (SVM–GP) Fz_max (N)	Model IV (SVM–RBF) Fz_max (N)	Model V (RFR) Fz_max (N)	Model VI (ANN) Fz_max (N)
1	Free	FlatEnd-R1	1422	1427.71	1268.28	1414.09	1347.1	1356.14	1379.59
2	Free	FlatEnd-R2	1287	1324.8	1303.51	1303.59	1274.25	1305.76	1283.35
3	Free	Hemispherical	1154	1221.74	1192.09	1178.2	1148.46	1195.96	1181.32
4	500	FlatEnd-R1	1311	1316.23	1173.27	1319.77	1315.28	1257.62	1281.88
5	500	FlatEnd-R2	1189	1213.31	1189.44	1212.01	1222.78	1239.04	1188.06
6	500	Hemispherical	1076	1110.26	1102.69	1098.02	1086.06	1121.32	1080.9
7	1000	FlatEnd-R1	1194	1204.74	1136.9	1199.7	1184.67	1096.7	1173.09
8	1000	FlatEnd-R2	1091	1101.82	1117.04	1103.02	1095.07	1093	1088.53
9	1000	Hemispherical	997	998.768	1027.04	1012.01	1016.88	1038.42	982.783
10	1500	FlatEnd-R1	1058	1093.25	1083.13	1080.95	1078.53	1046.94	1063.58
11	1500	FlatEnd-R2	978	990.331	1010.28	1001.11	1002.27	1015.72	992.001
12	1500	Hemispherical	908	887.279	889.085	939.538	1014.95	1017.38	893.899

The purpose of the training phase is to minimize error and to optimize accuracy. Hence, the training of the model is stopped once the minimum error value is obtained. Thereafter, test data is fed to the trained ANN model to forecast the output as illustrated by Fig. 8. The predicted outcomes of this model may be considered as accurate and reliable.

3 Results and discussion

3.1 Experimental results and analysis

The experimental and estimated results for maximum axial load (Fz_max) for various runs have been given in Table 4. Fig. 9a graphically depicts the impacts of the interactions of tool rotation speed and tool shape. It was observed that maximum axial load increased with the decrease in tool rotation speed. Lower tool speed resulted in a decrease in

Fig. 9 a Interaction of spindle speed and tool shape for axial peak load. **b** Chip-formation during run 12 (at spindle speed 1500 rpm, force 908 N)
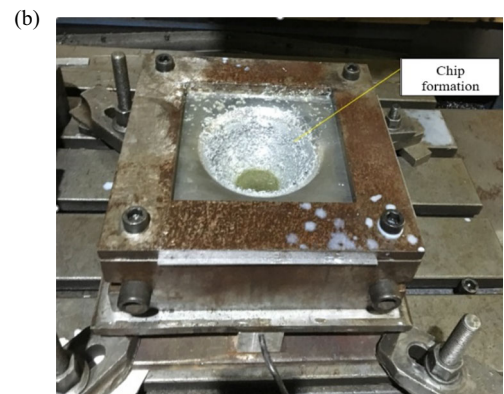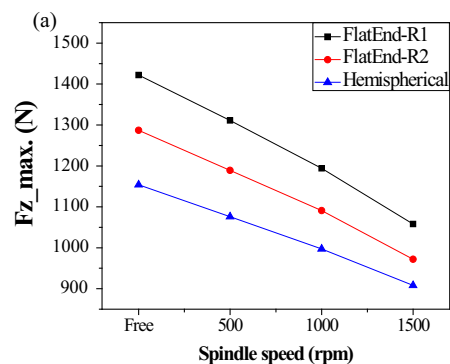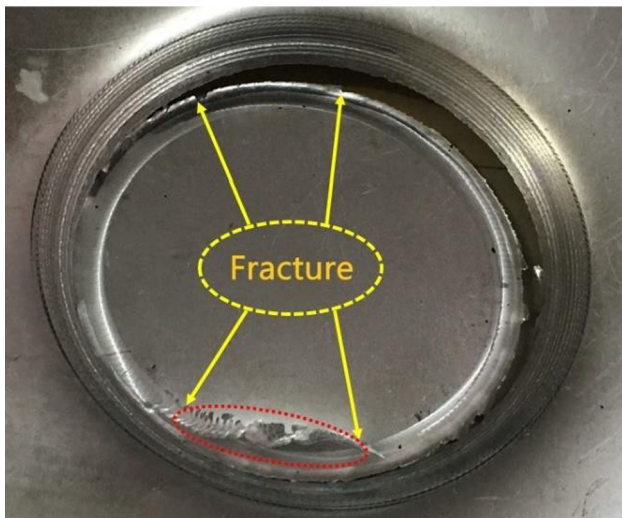
Fig. 10 Failure of specimen during run 10 (by Flatend-R1 tool shape, 1500 rpm spindle speed, force 1058 N, fracture height = 19.40 mm)

friction at forming area which further decreased the forming-temperature. The decrease in forming-temperature resulted in a reduction in ductility and formability of material and, hence, a higher amount of deforming load was desired. The axial load values were noticed to be highest when the tool was kept at "free-to-rotate" conditions for all levels of tool-shape because the friction was reduced to a minimal value. The use of higher spindle speed could decrease the desired load, but, at the expense of surface quality for all tool shapes because some material was removed in the form of chips (see Fig. 9b).

As far as the impact of tool shape is concerned, the forming forces were found to be greater when the flat-end tools were used as a forming agent in place of hemispherical-end tool. The combination of flat-end tool and lower spindle speed increased the forming forces drastically and can become the limiting factor for forming machine. Axial peak loads were decreased significantly when the greater spindle speed was used with hemispherical tool. Moreover, fracture in the components" happened when the higher spindle speed was employed along with Flatend-R1 tool at a height of 19.4 mm of the conical frustum because of excessive thinning and removing some material in the form of chips (see Fig. 10).

It was also noticed that as the tool shape was changed from hemispherical-end to Flatend-R1, the axial peak forces increased by 16.51%, 19.75%, 21.84%, and 23.22% for tool rotation speeds of 1500 rpm, 1000 rpm, 500 rpm, and "free-to-rotate" condition, respectively. It can also be noticed from the results that the increment of force was also found to raise as the tool rotation speed was decreased. Similarly, peak values of load were increased by 27.09%, 31.59%, and 34.4% for the hemispherical end, Flatend-R2, and Flatend-R1, respectively, when the tool rotation speed was decreased from 1500

rpm to "free-to-rotate" condition. It can also be noticed from the results that the increment of force was also found to raise as the side radius of the tool was decreased. When the condition of forming was changed from the combination of Flatend-R1 and "free-to-rotate"

condition to the combination of hemispherical-end and 1500 rpm, the forming force was found to decrease by 36.14% which is very significant to save power and energy.

3.2 Estimation of axial load values by ML methods

ML models have been executed of three ML techniques, (Matplotlib, Pandas, and Keras) by using Python 3.7.4 64-bit to create six different models. To estimate axial forming forces, four different variants of the SVM technique have been exploited along with the models of RFR and ANN. The SVM models have been preferred in literature for better results [29]. The literature also endorsed that the Gaussian Process (GP) Regression model is suitable for small training samples [27, 31] which the authors have investigated. Therefore, a comparative analysis has been performed between the predicted and experimental results of the three models for finding their accuracy. Figure 11 depicts the workflow for forecasting the axial load. The first step was to pre-process the experimental data for missing values before selecting features and transformation approaches. Once the dataset became ready, it was divided into two parts i.e., training data (80%) and test data (20%). Thereafter, the proposed model was trained on the training data samples and the model was fine-tuned using various parameters of the model to optimize the accuracy of the model. Furthermore, the trained model was used to predict the axial peak forces for the given run according to DOE. The axial load values predicted by all the models were matched with the actual load values and the accuracy of models were also analyzed.

3.3 ML models used for prediction of maximum axial force

Training and testing statistics of SVM variants are shown in Table 5. Four variants of SVM viz. linear, polynomial, Gaussian process and Radial Basis Function (RBF) have been designed deferring on a kernel and labeled as model 1, model 2, model 3, and model 4 respectively. The Random Forest Regression (RFR) model is

created and n estimators are set to 50 which means the forest consists of 50 trees. The training and testing accuracy of Random Forest Regression (model 5) are shown in Table 6.

Similarly, the ANN model has been trained and tested using the parameters vis-a-vis optimizer, activation function, number of nodes, and number of epochs which are presented in Table 7. In this model, an optimizer algorithm has been

Fig. 11 The workflow of ML models for the prediction of Fz_max
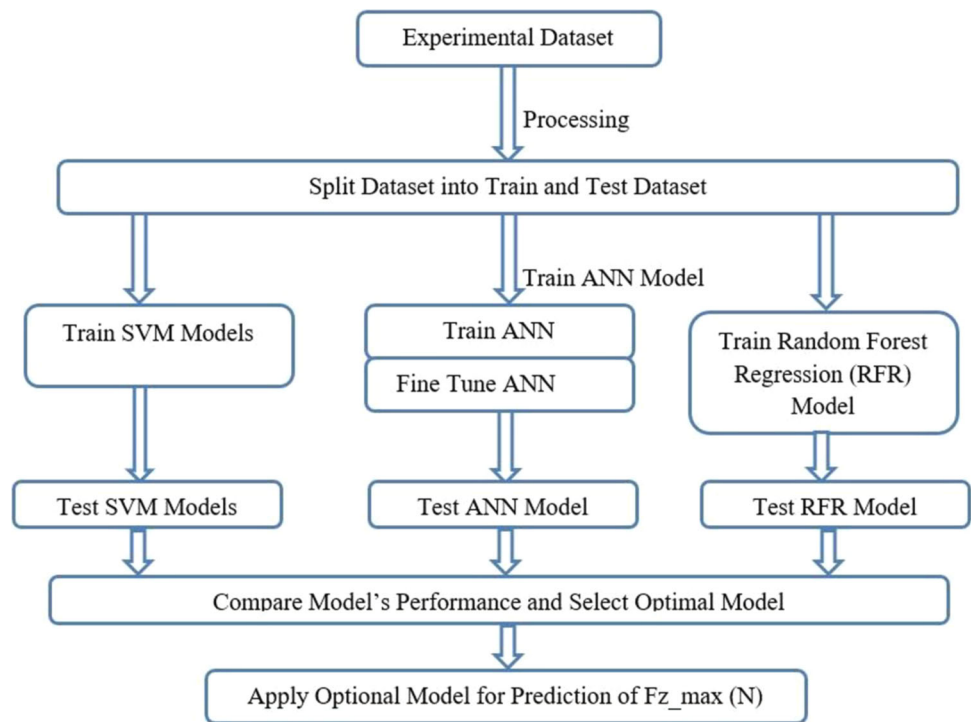
Table 5 MAPE, MSE, and R^2 during the training and testing of SVM models

Kernel Method	Model Number	During the training				During the testing			
		RMSE	MSE	R^2	MAPE	RMSE	MSE	R^2	MAPE
SVM–Linear	Model 1	20.056	407.056	0.960	16.481	19.71	388.81	0.97	14.47
SVM–Poly	Model 2	78.94	6232.70	0.70	47.90	43.90	1927.90	0.89	39.07
SVM–Gaussian Process	Model 3	11.33	128.38	0.97	13.11	16.24	264.04	0.98	13.85
SVM–RBF	Model 4	27.22	740.004	0.964	20.20	67.02	4492.60	0.74	51.66

Table 6 Training parameters for random forest regression (RFR) model (model 5)

Model number	During the training				During the testing			
	RMSE	MSE	R^2	MAPE	RMSE	MSE	R^2	MAPE
Model 5	40.301	1624.242	0.922	35.275	89.322	7978.425	0.553	85.573

Table 7 Training parameters and errors for ANN Model (model 6)

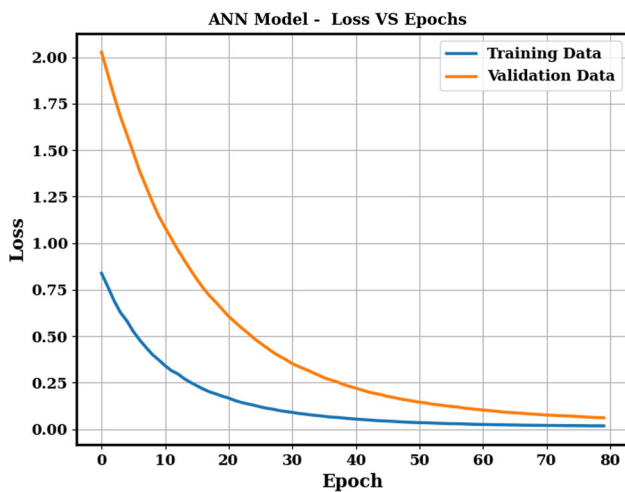| Optimizer	Activation	During the training						During the testing					
		Nodes	Epochs	RMSE	MSE	R^2	MAPE	Nodes	Epochs	RMSE	MSE	R^2	MAPE
SGD	Tanh	50	80	18.15	329.50	0.97	5.96	50	80	14.32	212.27	0.98	6.98

Fig. 12 ANN model–loss versus epochs

used to change the weights and learning rate to minimize the losses and to get the results at a faster rate. The activation function of a neuron defines the output of the neuron. The number of nodes indicates the total number of neurons in the artificial neural network. In the ANN model, one epoch indicates a full training cycle iteration on the training dataset. The parameters have been set to train the model for achieving higher accuracy and lower errors. The tensor flow of Keras has been used to implement ANN. The model has shown high training accuracy when it was explored using Stochastic Gradient Descent (SGD) optimizer, tanh activation function, and 50 nodes in the hidden layer. The tanh activation function is suitable for a small training sample size. The training and testing accuracies of the ANN model were found as 97% and 98%, respectively, and errors viz. the Root Mean Square Error (RMSE), Mean Square Error (MSE), R-Squared (R^2), and MAPE were calculated.

During the training of the ANN model, it was evident that the model produced higher accuracy and minimum loss at the 80th epoch. After this value, the increase in epoch did not affect accuracy significantly. The ANN model loss versus epochs is represented in Fig. 12 which shows that during the training of the model, there is a sharp decrease in the loss till the 30th epochs, and afterward, loss started decreasing gradually and produced the minimum loss at the 80th epoch. Furthermore, during the testing of this model, there was a sharp decrease in loss till the 40th epoch, and afterward, loss started reducing gradually and produced the minimum loss at the 80th epoch. The predicted accuracy of model 1 (SVM—Linear), model 2 (SVM–Poly), model 3 (SVM–Gaussian Process), model 4 (SVM – RBF), model 5 (RFR), and Model 6 (ANN) are shown in Fig. 13**(a)-(f)**, respectively which delineates that among the four SVM regression models, the best prediction accuracy was produced by Model 3—SVM Gaussian Process (which is 97%) whereas the ANN model

produced 98% prediction accuracy, which is slightly higher than SVM Gaussian Process model. The other models (model 2 (SVM–Poly), model 4 (SVM–RBF) and model 5 (RFR)) displayed lower prediction accuracy as compared with the model 3 (SVM–Gaussian Process) and model 6 (ANN).

3.4 Comparison of actual and predicted values of maximum load

Training accuracy of SVM models (refer to Table 4) clearly shows that SVM- Gaussian Process model outperforms the rest of SVM models because Gaussian regression is suitable for small training dataset [27]. The comparison of actual and estimated values of maximum load using SVM, RFR, and ANN is illustrated by Fig. 14. Table 8 depicted the comparison of the accuracy of SVM, RFR, and ANN models for predicting the axial peak forces for the defined process condition.

The comparison of the performance measures the Root Mean Square Error (RMSE), R-Squared (R^2), Mean Squared Error (MSE) and Mean Absolute Percentage Error (MAPE) of SVM- Gaussian Process, Random Forest, and ANN models which concluded that the accuracy of SVM-Gaussian Process (97%) is quite close to the ANN model (98%). However, the accuracy of the ANN model was found to be a bit higher than the SVM–Gaussian Process model because activation function, optimizer, and other features make the ANN model more robust and suitable for nonlinear problems. Moreover, the predicted result of the ANN model is very close to experimental values which can be considered evidence of the significance and efficiency of the ANN model.

Table 9 shows performance comparison with others work and delineates that MAPE accuracy of proposed ANN is slight better and model accuracy (R2) is 98%. Alsamhan et al. [46] had not mentioned computational time whereas this work also presented computational time. However, the material, experimental setup parameters and conditions were different in compared work. All the experiments were run on intel core i7 11th gen laptop with 16 GB RAM. Table 10 shows the computational time for each model during the training and test of the models. It is good to note that the computation time for running ANN (model 6) and SVM-Gaussian Process Model (model 3) were 1.002 seconds and 0.021 seconds. However, ANN model takes approximately 0.59 second more than SVM-Gaussian Process model that did not make any significant overhead in terms of computational time but ANN has slight better accuracy.

Thus, the proposed ML model viz. ANN and SVM- Gaussian Process can be used as an efficient tool to forecast the desired maximum deforming load in this dieless operation for reducing the cost of experimentation. Furthermore, a comparison of the predicted results of the proposed models also
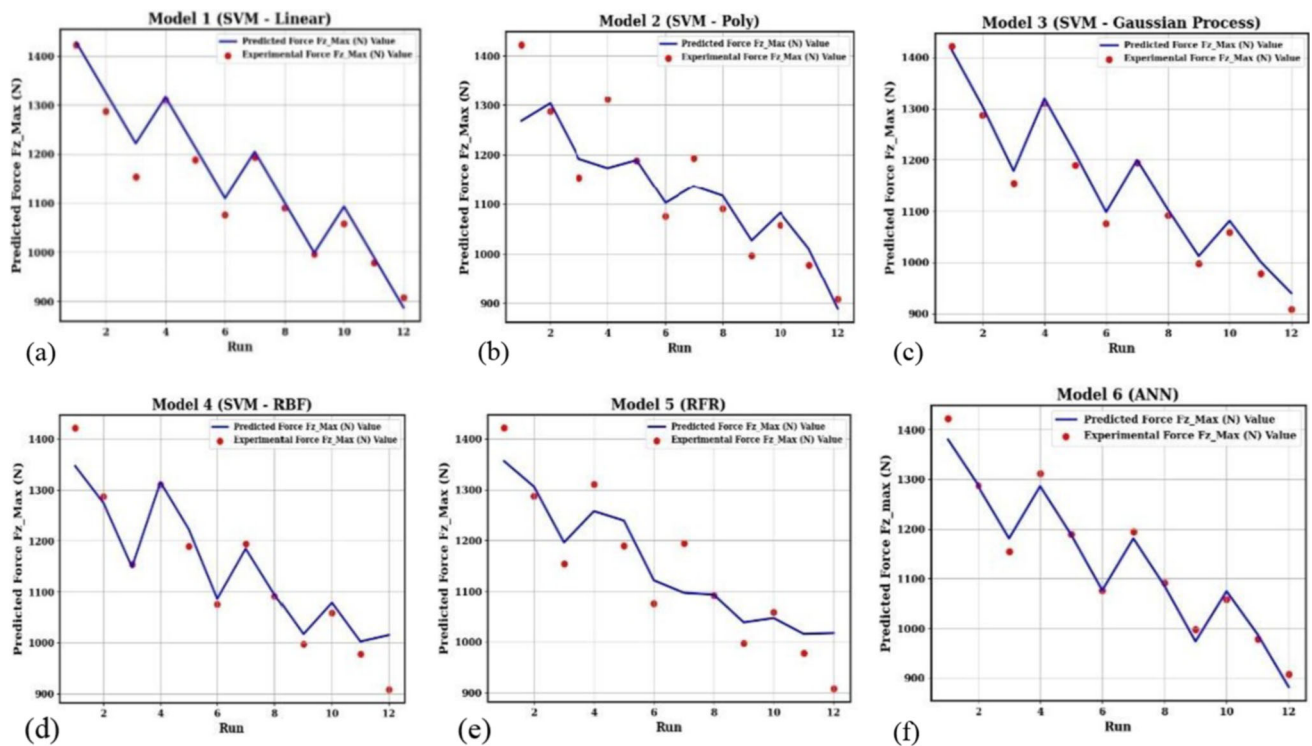
Fig. 13 a Prediction accuracy of model 1 (SVM—Linear). **b** Prediction accuracy of model 2(SVM—Ploy). **c** Prediction accuracy of model 3 (SVM—Gaussian Process). **d** Prediction accuracy of model 4 (SVM—RBF). **e** Prediction accuracy of model 5 (RFR). **f** Prediction accuracy of model 6 (ANN)
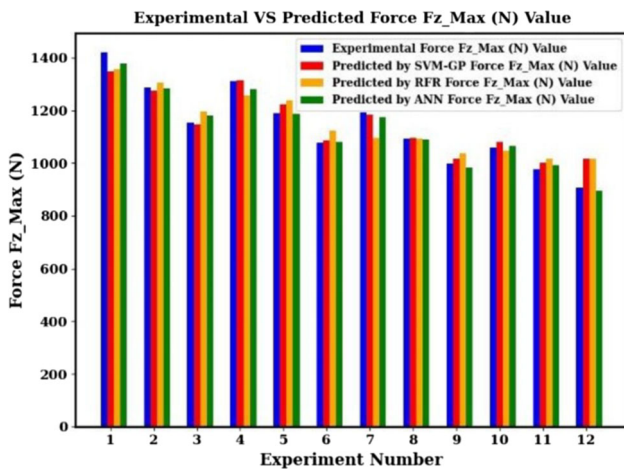
Fig. 14 Comparison between experimental and predicted axial forces

revealed that the ANN model has an advantage over the SVM model to predict the axial peak forces.

4 Conclusions

This work explored the impact and interactions of tool rotation and tool shape on axial peak deforming loads by experimental examinations during SPIF. Several machine learning techniques have been analyzed to forecast the load values. The conical frustums of constant wall angle were produced from AA7075-O sheets. The SVM, RFR, and ANN models were developed and trained (using specified levels of spindle speed and tool shape) on experimental data to predict the axial peak forces. The predicted values of maximum deforming load of all models were compared with actual measured values from experimentation to verify the accuracy and suitability of proposed models. The following conclusions have been made:

- The axial load values were noticed to be highest when the tool was kept at "free-to-rotate" conditions for all levels of tool-shape because the friction was reduced to a minimal value. The use of higher spindle speed could decrease the desired load, but, at the expense of surface quality for all tool shapes because some material was removed in the form of chips. As far as the impact of tool shape is concerned, the forming forces were found to be greater when the flat-end tools were used as a forming agent in place of hemispherical-end tool

- The combination of flat-end tool and lower spindle speed increased the forming forces drastically and can become the limiting factor for forming machine. Axial peak loads

Table 8 Comparison of prediction accuracy of SVM, RFR and ANN models

Sr. No.	Model	RMSE	MSE	R^2	MAPE
1	SVM-Gaussian process model (model 3)	19.30	372.67	0.97	17.73
2	Random forest regression model (model 5)	56.68	3212.78	0.84	47.84
3	ANN model (model 6)	19.24	370.19	0.98	4.96

Table 9 Performance comparison with others work

References	Model	Model accuracy (during training)		Parameters (during testing)		Computational time (in second)	
		MAPE		R^2	MAPE	R^2	
Alsamhan et al. [46]	ANN	8.89		NA	11.59	NA	NA
	ANFIS	6.42		NA	15.44	NA	NA
	Regression	16.27		NA	26.05	NA	NA
Current work	ANN	5.96		0.97	6.98	0.98	1.002
	SVM-GP	13.11		0.97	13.85	0.98	0.021

Table 10 Computation time in second during training and testing of the models

SVM–linear model 1	SVM–poly model 2	SVM–GP model 3	SVM_RBF model 4	RFR model 5	ANN model 6
0.013	0.071	0.021	0.058	0.042	1.002

were decreased significantly when the greater spindle speed was used with hemispherical tool

- When the condition of forming was changed from the combination of Flatend-R1 and "free-to-rotate" condition to the combination of hemispherical-end and 1500 rpm, the forming force was found to decrease by 36.14% which is very significant to save power and energy for producing the components

- The SVM-Gaussian Process and ANN models produced better accuracy as compared to other models. Moreover, the ANN model outperforms the SVM-Gaussian Process with greater accuracy of prediction (98%). Moreover, a comparison of the predicted results of proposed models also revealed that the ANN model has an advantage over the SVM model for predicting axial peak forces

Hence, the proposed ML model viz. ANN and SVM—Gaussian Process can be used as an efficient tool to forecast the desired maximum deforming load in this dieless operation for reducing the cost of experimentation. The predicted result of the ANN model was closed to the experimental result and the model can successfully be implemented to explore the different process conditions for a variety of materials. Furthermore, the secure and effective employment of required machinery and auxiliary hardware can be promised by estimating peak deforming loads using machine learning techniques which offer an alternative economical, easy,

and technology-based solution to the cumbersome experimental process of this die-less approach of forming. Future work would focus on the investigation of different materials and input conditions to forecast the deforming load and to develop hybrid models for complex process conditions using ML techniques during the ISF process.

Declarations

References

1. Liu, Z., Cheng, K., Peng, K.: Exploring the deformation potential of composite materials processed by incremental sheet forming: a review. Int. J. Adv. Manuf. Technol. **118**, 2099–2137 (2022)
2. Kumar, A., Gulati, V.: Experimental investigation and optimization of surface roughness in negative incremental forming. Measurement **131**, 419–430 (2019)
3. Zhu, H., Liu, L., Liu, Y.: Research on the selective multi-stage two-point incremental forming based on the forming angle. J. Mech. Sci. Technol. **35**, 3643–3658 (2021)
4. Afzal, M.J., Hajavifard, R., Buhl, J.: Influence of process parameters on the residual stress state and properties in disc springs

made by incremental sheet forming (ISF). Forsch. Ing. **85**, 783–793 (2021)

5. Jeswiet, J., Micari, F., Hirt, G.A., Bramley, J.D., Allwood, J.: Asymmetric single point incremental forming of sheet metal. CIRP Ann. **54**(2), 88–114 (2005)

6. Kumar, A., Mittal, R.K.: Incremental Sheet Forming Technologies: Principles, Merits, Limitations, and Applications. CRC Press (2020)

7. Zhu, H., Wang, Y., Kang, J.: The effect of extrusion direction on the forming quality in CNC incremental forming with multidirectional adjustment of sheet posture. J. Mech. Sci. Technol. **35**, 1671–1679 (2021)

8. Zhu, H., Ou, H., Popov, A.: Incremental sheet forming of thermoplastics: a review. Int. J. Adv. Manuf. Technol. **111**, 565–587 (2020)

9. Centeno, G., Bagudanch, I., Jesús, A.M.D., Maria, L.G.R., Vallellano, C.: Critical analysis of necking and fracture limit strains and forming forces in single-point incremental forming. Mater. Des. **63**, 20–29 (2014)

10. Kurra, S., Bagade, S.D., Regalla, S.P.: Deformation behavior of extra deep drawing steel in single-point incremental forming. Mater. Manuf. Process. **30**(10), 1202–1209 (2015)

11. Kumar, A., Gulati, V., Kumar, P., Singh, V., Kumar, B., Singh, H.: Parametric effects on formability of AA2024-O aluminum alloy sheets in single point incremental forming. J. Market. Res. **8**(1), 1461–1469 (2019)

12. Magdum, R.A., Chinnaiyan, P.: A critical review of incremental sheet forming in view of process parameters and process output. Adv. Mater. Process. Technol. **8**(2), 2039–2068 (2022)

13. Kumar, A., Gulati, V., Kumar, P., Singh, H.: Forming force in incremental sheet forming: a comparative analysis of the state of the art. J. Braz. Soc. Mech. Sci. Eng. **41**(6), 251 (2019)

14. Yang, Z., Chen, F., Gatea, S.: Design of the novel hot incremental sheet forming experimental setup, characterization of formability behavior of polyether-ether-ketone (PEEK). Int. J. Adv. Manuf. Technol. **106**, 5365–5381 (2020)

15. Oraon, M., Mandal, S., Sharma, V.: Predicting the deformation force in the incremental sheet forming of AA3003. Mater. Today: Proc. **45**, 5069–5073 (2021)

16. Bansal, A., Lingam, R., Yadav, S.K., Reddy, N.V.: Prediction of forming forces in single point incremental forming. J. Manuf. Process. **28**, 486–493 (2017)

17. Kurra, S.: Experimental study on force measurement for AA 1100 sheets formed by incremental forming. Mater. Today: Proc. **18**, 2738–2744 (2019)

18. Liu, F., Yanle, L., Zinan, C., Wang, Z., Fangyi, L., Jianfeng, L.: Preliminary modelling of forming forces in three directions for incremental sheet forming process based on the contact area. Procedia Manuf. **50**, 630–636 (2020)

19. Sebastian, W., Marlon, H., Andreas, D., Wolfgang, T., Dominic, S., Nelson, F.L.D., Tekkaya, A.E.: Force reduction by electrical assistance in incremental sheet-bulk metal forming of gears. J. Mater. Process. Technol. **296**, 117194 (2021)

20. Hussain, G., Mohammed, A.: Analysis of wall curling in incremental forming of a sheet metal: role of residual stresses, stretching force and process conditions. J. Market. Res. **11**, 1548–1558 (2021)

21. Liu, Z., Li, Y.: Small data-driven modeling of forming force in single point incremental forming using neural networks. Eng. Comput.Comput. **36**(4), 1589–1597 (2020)

22. Kumar, A., Gulati, V.: Experimental investigations and optimization of forming force in incremental sheet forming. Sādhanā **43**(10), 159 (2018)

23. Kumar, A., Gulati, V.: Optimization and investigation of process parameters in single point incremental forming. Indian J. Eng. Mater. Sci. **27**, 246–255 (2020)

24. Zhidong, C., Ming, L., Chen, J.: Analytical modeling and experimental validation of the forming force in several typical incremental sheet forming processes. Int. J. Mach. Tools Manuf **140**, 62–76 (2019)

25. Oleksik, V., Adrian, P., Adinel, G., Mihaela, O.: Experimental studies regarding the single point incremental forming process. Acad. J. Manuf. Eng. **8**, 51–56 (2010)

26. Fiorentino, A., Elisabetta, C., Aldo, A., Luca, M., Claudio, G.: Analysis of forces, accuracy and formability in positive die sheet incremental forming. Int.J. Mater. Form. **2**(1), 805 (2009)

27. Nian, Z., Xiong, J., Zhong, J., Leatham, K.: Gaussian process regression method for classification for high-dimensional data with limited samples. In: Eighth International Conference on Information Science and Technology (ICIST), IEEE. 358–363, (2018)

28. William, N.S.: What is a support vector machine? Nat. Biotechnol. **24**(12), 1565–1567 (2006)

29. Jae, M.H., Lee, Y.C.: Bankruptcy prediction using support vector machine with optimal choice of kernel function parameters. Expert Syst. Appl. **28**(4), 603–614 (2005)

30. Lingjian, Y., Liu, S., Tsoka, S., Papageorgiou, L.G.: A regression tree approach using mathematical programming. Expert Syst. Appl. **78**, 347–357 (2017)

31. Joaquin, Q.C., Rasmussen, C.E., Williams, C.K.: Approximation methods for Gaussian process regression. In: Bottou, L., Chapelle, O., DeCoste, D., Weston, J. (eds.) Large-Scale Kernel Machines, pp. 203–223. MIT Press, Cambridge (2007)

32. Mohamed, Z.E.: Using the artificial neural networks for prediction and validating solar radiation. J. Egypt. Math. Soc. **27**(1), 1–13 (2019)

33. Jalal, M., Grasley, Z., Gurganus, C., Bullard, J.W.: A new nonlinear formulation-based prediction approach using artificial neural network (ANN) model for rubberized cement composite. Eng. Comput.Comput. **38**, 283–300 (2022)

34. Jain, A.K., Mao, J., Mohiuddin, K.M.: Artificial neural networks: a tutorial. Computer **29**(3), 31–44 (1996)

35. Khan, S.U., Ayub, T., Rafeeqi, S.: Prediction of compressive strength of plain concrete confined with ferrocement using artificial neural network (ANN) and comparison with existing mathematical models. Am. J. Civ. Eng. Archit. **1**(1), 7–14 (2013)

36. Raed, J., Shahrour, I., Juran, I.: Application of artificial neural networks (ANN) to model the failure of urban water mains. Math. Comput. Model. **51**(9–10), 1170–1180 (2010)

37. Indu, K., Shrivastava, V.K.: A survey of big data in healthcare industry. In: Choudhary, R., Mandal, J., Auluck, N., Nagarajaram, H. (eds.) Advanced Computing and Communication Technologies, pp. 245–257. Springer, Singapore (2016)

38. Gérard, B.: Analysis of a random forests model. J. Mach. Learn. Res. **13**(1), 1063–1095 (2012)

39. Saqib, A., Nasr, M.M., Alkahtani, M., Altamimi, A.: Predicting surface roughness and exit chipping size in BK7 glass during rotary ultrasonic machining by adaptive neuro-fuzzy inference system (ANFIS). In: Proceedings of the International Conference on Industrial Engineering and Operations Management, (2017)

40. Kurra, S., Rahman, N.H., Regalla, S.P., Gupta, A.K.: Modeling and optimization of surface roughness in single point incremental forming process. J. Market. Res. **4**(3), 304–313 (2015)

41. Khan, M.S., Coenen, F., Dixon, C., Subhieh, E.S., Penalva, M., Rivero, A.: An intelligent process model: predicting springback in single point incremental forming. Int. J. Adv. Manuf. Technol. **76**(9–12), 2071–2082 (2015)

42. Racz, S.G., Breaz, R.E., Bologa, O., Tera, M., Oleksik, V.S.: Using an adaptive network-based fuzzy inference system to estimate the vertical force in single point incremental forming. Int. J. Comput. Commun. Control **14**(1), 63–77 (2019)

43. Jawale, K., Duarte, J.F., Reis, A., Silva, M.B.: Microstructural investigation and lubrication study for single point incremental

forming of copper. Int. J. Solids Struct. **151**, 145–151 (2018). https://doi.org/10.1016/j.ijsolstr.2017.09.018

44. Oraon, M., Sharma, V.: Predicting force in single point incremental forming by using artificial neural network. Int. J. Eng. **31**(1), 88–95 (2018). https://doi.org/10.5829/ije.2018.31.01a.13

45. Oraon, M., Sharma, V.: Prediction of surface roughness in single point incremental forming of AA3003-O alloy using artificial neural network. Int. J. Mater. Eng. Innov. **9**(1), 1–19 (2018). https://doi.org/10.1504/IJMATEI.2018.092181

46. Alsamhan, A., Ragab, A.E., Dabwan, A., Nasr, M.M., Hidri, L.: Prediction of formation force during single-point incremental sheet metal forming using artificial intelligence techniques. PLoS ONE **14**(8), e0221341 (2019)

47. Li, Z., He, S., Zhang, Y., An, Z., Gao, Z., Lu, S.: Numerical prediction of Joule heating effect in electric hot incremental sheet forming. Int. J. Adv. Manuf. Technol. **121**(11–12), 8221–8230 (2022)

48. Li, W., Essa, K., Li, S.: A novel tool to enhance the lubricant efficiency on induction heat-assisted incremental sheet forming of Ti-6Al-4 V sheets. Int. J. Adv. Manuf. Technol. **120**(11–12), 8239–8257 (2022)

49. Najm, S.M., Paniti, I.: Investigation and machine learning-based prediction of parametric effects of single point incremental forming on pillow effect and wall profile of AlMn1Mg1 aluminum alloy sheets. J. Intell. Manuf. **34**(1), 331–367 (2023)